Sedimentation of gas-fluidized particles with random shape and size

Laurence Girolami*
Laboratoire GéHCO, Campus Grandmont, Université de Tours, 37200 Tours, France

Frédéric Risso†
Institut de Mécanique des Fluides de Toulouse (IMFT), Université de Toulouse, CNRS, 31400 Toulouse, France

(Received 4 March 2019; published 3 July 2019)

This work deals with the fluidization and sedimentation of fine solid particles, of random shape and size, similar to those commonly involved in geophysical mass flows, such as pyroclastic flows. While heated to avoid the effect of moisture and the formation of clusters, particles were first uniformly fluidized by a hot gas flow, up to a high expansion rate, and then sedimented after stopping the gas supply. Three different materials are explored, involving contrasted geometries, each characterized by a specific particle volume fraction at packing Φ_{pack}. Within the range of values of the solid volume fraction $\Phi_s/\Phi_{\text{pack}}$ studied here, the dense suspension forms a fully fluidized homogeneous mixture, with no segregation, for which the fluidization and sedimentation velocities are equal. Despite a significant discrepancy between the intrinsic properties of the different materials used, all measured velocities are observed to collapse into a single master curve $f(\Phi_s/\Phi_{\text{pack}})$ provided that they are normalized by the relevant scaling. Regarding the sedimentation velocity, Φ_{pack} turns out to be sufficient to characterize the material made with a random distribution in particle shape and size.

DOI: 10.1103/PhysRevFluids.4.074301

I. INTRODUCTION

Fluidization processes are largely developed in both geophysical mass flows and industrial processes in which a swarm of heavy particles is suspended by an upward fluid flow and settles once this flow vanishes. Far from the boundaries, the fluidization and sedimentation processes are considered to be equivalent; the fluidization velocity U_f, which maintains the particles at zero average velocity, is expected to be the same as the settling velocity U_{sed} at which the particles fall when the fluid is at rest. Predicting these velocities represents an important step for the modeling of a wide range of both natural and industrial systems that involve similar suspensions of particles and gas. Many efforts have been previously devoted to the determination of U_f in fluidized beds [1–3] as well as U_{sed} in sedimenting suspensions [4,5]. For the simplest case of a population of monodisperse spherical particles, U_f and U_{sed} are found to depend on the fluid properties (its density ρ_f and viscosity μ_f), the particles properties (its density ρ_s and diameter d), the mixture properties (its particle volume fraction Φ_s), and the gravitational acceleration g [1,2]. Otherwise, when the particles involved in the mixture are not spherical, their size can be characterized by the diameter of a sphere of the same volume ϑ, such as $d = (6\vartheta/\pi)^{1/3}$, as defined hereafter in this paper. Furthermore, in more common situations such as those encountered in both natural and industrial systems, the dense

*laurence.girolami@univ-tours.fr
†frisso@imft.fr

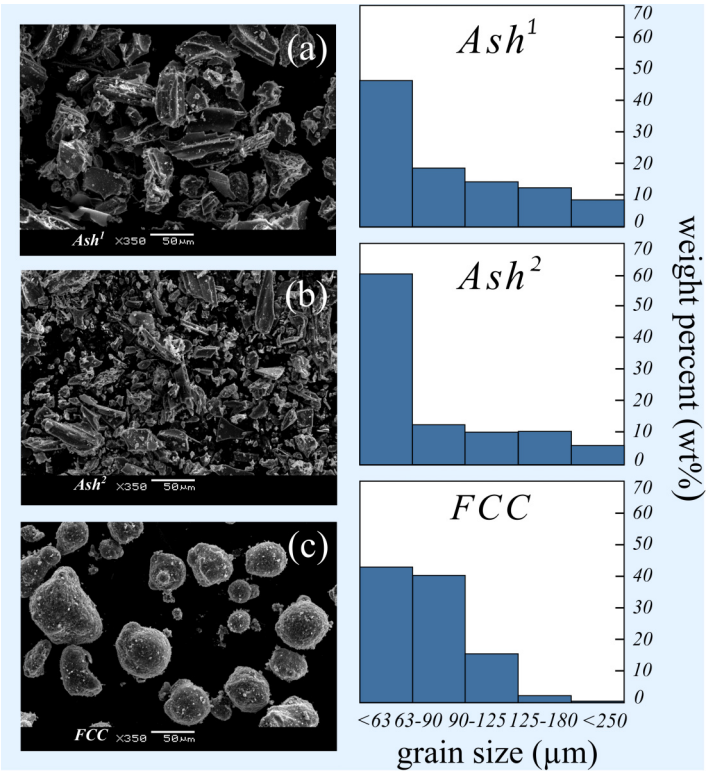

FIG. 1. Pictures and size distributions of Ash^1, Ash^2, and FCC.

suspension usually involves a polydisperse material which makes the mixture behavior dependent on the particle size and shape distributions. Previous scientific achievements, conducted by one of the authors [6–9], have reported experimental measurements of U_f and U_{sed} for gas-solid mixtures involving both natural and synthetic materials made of volcanic ash and fluid catalytic cracking. These works focused on the dam-break flow of hot dense suspensions and highlighted that the sedimentation velocity plays a major role in the runout duration of basal pyroclastic flows generated by explosive eruptions, such as the gravitational collapse of a lava dome. However, they did not manage to gather the results involving U_f and U_{sed}, which were found to depend on the considered sample of particles. The present work revisits these experimental data and shows that a different scaling allows one to match both the fluidization and sedimentation velocities obtained with two different ash samples [Ash^1 and Ash^2; Figs. 1(a) and 1(b)] with those of more spherical synthetic particles (FCC) of comparable size distribution but of contrasted geometry [Fig. 1(c)].

Scanning electron microscopy photographs of the single sample are exposed in Fig. 1 and show that Ash^1 and Ash^2 display various complex anisotropic shapes, whereas FCC are almost spherical. The particles properties and the experimental operating conditions are exposed in Table I, while the particles size distributions, in percent of weight, are provided in Table II and illustrated in Fig. 1.

II. EXPERIMENTAL PROCEDURE

The present investigation is based on classical experiments of both fluidization and sedimentation that were conducted using conventional experimental techniques. Therefore, the procedures are briefly described here while focusing on the conditions necessary to get a homogeneous mixture

TABLE I. Experimental parameters for the different materials Ash[1], Ash[2], and FCC.

Experimental parameters	Ash[1]	Ash[2]	FCC
Solid particle density ρ_s (kg m^{-3})	1600	1490	1420
Mean particle equivalent diameter d (μm)	80	65	71
Particle volume fraction at packing ϕ_{pack}	0.58	0.60	0.484
Range of particle volume fraction ϕ_s	0.38–0.58	0.40–0.60	0.39–0.49
Range of dilatation rate $E = \frac{\phi_{\text{pack}}}{\phi_s}$	1.06–1.50	1.05–1.50	1.05–1.22
Minimum fluidization velocity U_{mf} (cm s^{-1})	0.32	0.17	0.26
Minimum bubbling velocity U_{mb} (cm s^{-1})	0.96	0.64	0.54
Fluidization group of Geldart [10] at 20 °C	C	C	A
Fluidization group of Geldart [10] at 180 °C	A	A	A

without segregation. Figure 2 shows the experimental configuration and the different flow regimes. The reservoir has a rectangular cross section, 150×300 mm^2, much larger than the particle size (<250 μm). Experiments have been performed at a temperature of 180 °C in order to prevent the cohesive effect and agglomeration induced by moisture. First, the hot particles were poured into the reservoir and fluidized by a hot gas, injected from a sintered stainless-steel porous plate located at the base. The mixture was stirred during the early stages of fluidization, in order to prevent the gas channeling, and thus let to expand freely and homogeneously until its maximum rate before cutting the gas injection. The initial state was obtained when all particles had settled down to the reservoir bottom until forming a random loose-packing deposit of thickness h_p and of solid volume fraction Φ_{pack}, measured with an accuracy of $\pm 2\%$. Fluidization experiments were carried out by injecting gas at superficial velocity U_f, measured by the means of flow meters with an accuracy of $\pm 1\%$. Increasing U_f first amounts to proportionally increasing the pressure drop across the static bed while Φ_s remains equal to Φ_{pack}. Above the threshold of minimum fluidization velocity U_{mf}, the bed starts to expand and the pressure drop becomes independent of U_f such as maintaining its maximum value. The bed remains homogeneously fluidized provided that U_f is inferior to U_{mb}, beyond which the nucleation of gas bubbles makes the mixture unstable. It is worth mentioning that this homogeneous regime of fluidization is characteristic of fine and slightly cohesive powders, termed *Group A* in the Geldart classification [10]. Therefore, it cannot be obtained with other types of particles, such as coarse and/or dense materials, termed *Groups B* and *D* [10], for which $U_{mf} \simeq U_{mb}$; or fine, cohesive powders, termed *Group C* [10], for which no real fluidization is observed except when heated at temperatures high enough to avoid the adsorbed moisture [6,7], as operated here. The present study reports measurements within the range of values obtained from U_{mf} to U_{mb}. Sedimentation experiments were carried out by stopping the gas injection once the suspension had reached a given expanded thickness h_0, corresponding to a given solid volume fraction Φ_s. A remarkable feature of these materials, when operated at high temperature, is their expandable properties. Here, the expansion rate, $E = h_0/h_p = \Phi_{\text{pack}}/\Phi_s$, is varied from 1.05 to 1.5. In this range, no segregation took place during either the fluidization or the sedimentation stage, such that the volume fraction

TABLE II. Granulometric distribution. The symbol † means that the fraction is given for the interval 63-0 μm.

Size range (μm)	250-180	180-125	125-90	90-63	63-45	45-32	32-0
Ash[1] (wt %)	8.44	12.36	14.26	18.67	46.27†		
Ash[2] (wt %)	6.09	10.51	10.41	12.72	60.27†		
FCC (wt %)	0.05	2.01	15.35	39.95	26.36	11.27	5.01

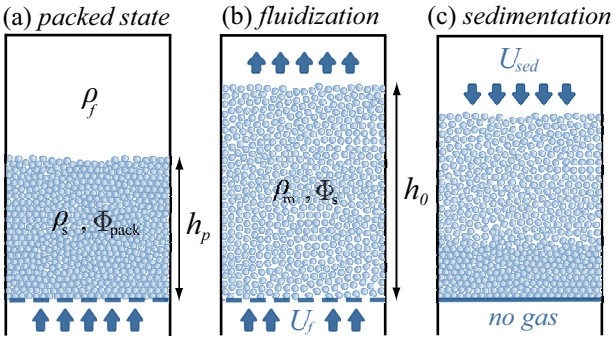

FIG. 2. Fluidization and sedimentation processes applied to a bed of particles: (a) the packed state ($U_f < U_{mf}$), (b) the homogeneous fluidization associated with a uniform bed expansion ($U_{mf} < U_f < U_{mb}$), (c) the sedimentation process obtained after cutting the gas supply ($U_{\rm sed} = U_f$).

Φ_s (measured with an accuracy of $\pm 2\%$) remains representative of the entire uniform mixture. This lack of segregation can be explained by the fact that the particle concentration in the mixture is always larger than 65% of the loose packing, which makes it difficult for the finest particles to move through the bed. Moreover, no size segregation is usually developed in well-sorted materials where each subset of particles is characterized by a value of U_{mf} that does not differ too much from that of the others, as observed here and previously described by Ref. [11]. Finally, $U_{\rm sed}$ was obtained (with an accuracy of $\pm 3\%$) from the time taken for the bed surface to deflate, from h_0 to h_p. After sedimentation, the deposit returns to the same initial volume fraction $\Phi_{\rm pack}$, indicating that this particular loose packing is a characteristic state of each sample which probably keeps memory of the sedimentation process in terms of particle arrangement and orientation.

III. RESULTS AND DISCUSSION

Gray symbols in Fig. 3 represent the measured fluidization velocities U_f (light gray) as well as the sedimentation ones $U_{\rm sed}$ (dark gray) as a function of the solid volume fraction Φ_s, for the three different samples, while white symbols indicate the measured minimum fluidization velocity U_{mf}. It turns out that $U_f = U_{\rm sed}$ for all the measurements performed at $U_f > U_{mf}$ ($\Phi_s < 0.95\,\Phi_{\rm pack}$), which is expected in the absence of vertical walls where the fluidization and sedimentation processes are identical except for a Galilean change of reference frame. The presence of side walls makes the situation different since the mean relative velocity of the particles is zero in the case of fluidization and amounts to $U_{\rm sed}$ in that of sedimentation. In this latter case, the mixture Reynolds number based on the bed width w, $\mathrm{Re} = \rho_m U_{\rm sed}\, w/\mu_m$, exceeds 1000, while the aspect ratio between the bed height and width is about unity. The mixture density ρ_m and viscosity μ_m, involved in this expression, will be defined later. For an initially homogeneous mixture, the boundary layers are therefore expected to remain confined near the side walls, while the flow profile remains flat over the major part of the reservoir cross section. Otherwise, in the case of fluidization, the gas Reynolds number based on the reservoir width is only a few tens. However, the gas flows through a dense bed of particles on average at rest, in the manner of a porous medium, where the pore size is negligible compared to the bed width, which explains that the influence of the side walls is negligible.

This fundamental finding allows us to no longer distinguish U_f from $U_{\rm sed}$ in the remainder of this paper, henceforth referred as U. Moreover, the particulate Reynolds number defined as $\mathrm{Re} = d\,U/\mu_f$ is lower than 0.03 in all experiments. For each sample, U is observed to decrease, following a constant negative slope, with increasing Φ_s without including the nonaligned threshold velocity U_{mf}. This observation highlights the presence of a transitional regime that distinguishes the fully fluidized suspensions ($\Phi_s < 0.95\Phi_{\rm pack}$) from the partly fluidized ones ($\Phi_s \simeq \Phi_{\rm pack}$) in which

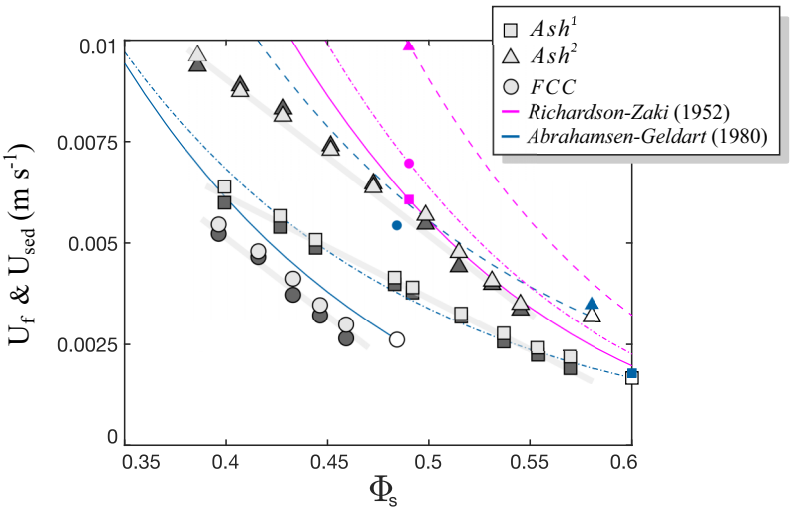

FIG. 3. Fluidization velocity U_f (light-gray symbols, measured with an accuracy of $\pm 1\%$) and sedimentation velocity U_{sed} (dark-gray symbols, measured with an accuracy of $\pm 3\%$) as a function of the particle volume fraction Φ_s (measured with an accuracy of $\pm 2\%$). White symbols represent U_{mf}, while blue and pink symbols indicate, respectively, the predictions of Ergun (1952) [12] and Richardson and Zaki (1954) [1] for U_{mf}.

macroscopic jamming frameworks induced by both interparticle and particle-wall interactions are developed and play a major role in the mixture dynamics, as observed in granular column collapses initiated from the dense to the loosely packed state [13]. Moreover, the results of the three different samples are observed to be significantly different, even for those obtained with the two samples of volcanic ash, highlighting a lack of universal gathering.

Many approaches have been addressed in the literature to overcome this gap. The minimum fluidization velocity is commonly described by the Ergun correlation [12],

$$U_{mf} = \frac{g(\rho_s - \rho_f)d^2}{150\,\mu_f}\left[\frac{(1-\Phi_{\text{pack}})^3}{\Phi_{\text{pack}}}\right], \tag{1}$$

which was established from a series of measurements performed in packed beds of spherical particles that were sedimented after being fluidized, similarly to the procedure followed in the present study. The predictions of Eq. (1) are represented by blue symbols in Fig. 3. Despite a surprisingly good agreement observed for the two samples of nonspherical particles (Ash^1 and Ash^2), Eq. (1) fails to predict that of the quasispherical powders (FCC). An evolution of U extended to the entire fluidized regime above U_{mf} has thus been proposed by [2],

$$U = U_{mf} + \frac{g(\rho_s - \rho_f)d^2}{210\,\mu_f}\left[\frac{(1-\Phi_s)^3}{\Phi_s} - \frac{(1-\Phi_{\text{pack}})^3}{\Phi_{\text{pack}}}\right]. \tag{2}$$

The predictions of Eq. (2), calculated from our experimental values of U_{mf}, are represented by blue (full and dashed) lines. The resulting curves are quantitatively not so far from the experimental measurements since they were initiated from identical values of U_{mf}, but fail anyway to reproduce the linear behavior, especially for Ash^1. Another famous expression, commonly used in both fluidization and sedimentation literatures, is that introduced by Richardson and Zaki [1] while considering the Stokes regime of dense suspensions,

$$U = \frac{g(\rho_s - \rho_f)d^2}{18\,\mu_f}(1-\Phi_s)^{4.65}. \tag{3}$$

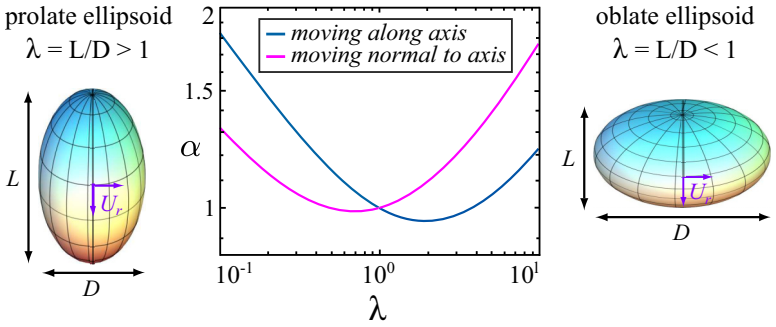

FIG. 4. Correction coefficient α accounting for the nonsphericity of the particles in the Stokes drag force as a function of the particle aspect ratio λ.

The predictions of Eq. (3), represented by the pink (full and dashed) lines in Fig. 3, disagree with the present experiments both in terms of magnitude and evolution trends. Therefore, the velocity scale, $g(\rho_s - \rho_f)d^2/\mu_f$, which is generally considered as the relevant one in the literature, does not allow one to collapse the present results. With the aim of attempting to determine the relevant scaling, we consider that the sedimentation of a particle within a concentrated fluidized suspension is equivalent to that described in a homogeneous fluid of density $\rho_m = \Phi_s\rho_s + (1 - \Phi_s)\rho_f$ and viscosity μ_m. The equation of motion written for the considered particle, falling at velocity U in the equivalent fluid, is given by the balance between the buoyancy and the drag forces:

$$g(\rho_s - \rho_m)\frac{\pi}{6}\,d^3 = 3\,\alpha\,\pi\,\mu_m\,d\,U, \tag{4}$$

where α is a prefactor derived from the Stokes drag force to account for the possible effect of the nonsphericity of the particles. Theoretical values of α are known for either oblate or prolate axisymmetric ellipsoids moving parallel or normal to their principal axis [14]. Figure 4 shows its value as a function of the particle aspect ratio λ and it turns out to remain close to unity, even for a rather pronounced gap to sphericity, which leads us to reasonably assume that $\alpha = 1$ in what follows.

Thus, Eq. (4) can be rewritten as

$$\frac{\mu_m}{\mu_f} = \frac{U_{\text{ref}}}{U}, \tag{5}$$

$$\text{taking} \quad U_{\text{ref}} = \frac{g(\rho_s - \rho_m)d^2}{18\,\mu_f}. \tag{6}$$

Note that the same relation is obtained from Eq. (4) by simultaneously considering a density contrast of $(\rho_s - \rho_f)$ for the buoyancy, and the relative average velocity between the gas and the particles of $U/(1 - \Phi_s)$ for the drag force.

It is important to note that Eq. (4) assumes that the particle under consideration is immersed in a homogenous fluid of uniform density and viscosity. This assumption is correct for a large particle falling through a suspension of small particles, but becomes questionable for a test particle of the same size as the particles in the suspension. Because the particles cannot overlap, there is necessarily a lack of particles in the vicinity of the test particle. The mixture density therefore varies with the distance from the test particle and amounts to that of the gas density in the vicinity of the particle and tends to the average mixture density at large distance. Moreover, the flow past the test particle experiences a nonlocal rheology because the length scale of the microstructure of the suspension is not small compared with the length scale of the flow, both being of the order of the particle size [15]. Here we can underline that the viscosity that appears in Eqs. (4)–(6) does not correspond to the

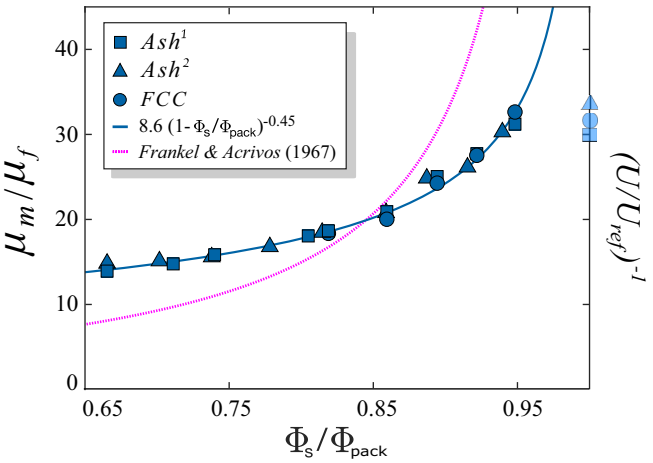

FIG. 5. Apparent bulk viscosity of the suspension normalized by the gas viscosity μ_m/μ_f (determined with an accuracy of $\pm 6\%$), which is the same as the inverse normalized sedimentation velocity $(U/U_{\text{ref}})^{-1}$, as a function of normalized solid volume fraction $\Phi_s/\Phi_{\text{pack}}$. Light-blue symbols represent the values at U_{mf}. $\Phi_s/\Phi_{\text{pack}}$ is determined with an accuracy of $\pm 1\%$, while μ_m/μ_f have an accuracy of $\pm 6\%$.

macroscopic average viscosity of the suspension, but represents a viscosity scale that is relevant to introduce U_{ref} as a reference velocity scale for both fluidization and sedimentation.

Figure 5 highlights that the measured sedimentation velocities, acquired with the three different samples, perfectly collapse into a single master curve when plotted in its dimensionless form μ_m/μ_f (or U_{ref}/U) as a function of the relevant mixture volume fraction $\Phi_s/\Phi_{\text{pack}}$ and drives us to draw two major conclusions. First, the characteristic velocity U_{ref}, built on the density contrast $(\rho_s - \rho_m)$, provides the correct scaling for sedimentation (and fluidization) velocities of dense suspensions, when generated in the homogeneous particulate regime of fluidization. Second, the value of Φ_{pack} is sufficient to characterize the size and shape distributions of the samples in regard to the determination of U.

Without forgetting the reservations made regarding the nature of the mixture viscosity introduced in this work, it is nonetheless interesting to compare it with previous models of suspension viscosity, especially to examine if they might follow a similar scaling law. Since the pioneering work of Einstein, many efforts have been devoted to the determination of the bulk viscosity of a dense suspension (see [16] and references therein), which usually propose expressions involving the solid volume fraction Φ_s and its value at packing, Φ_{pack}. For example, [17] derived a theoretical relation for a suspension of spheres which is based on the dissipation of the interstitial fluid between the particles,

$$\frac{\mu_m}{\mu_f} = \frac{9}{8}\left[\frac{\left(\frac{\Phi_s}{\Phi_{\text{pack}}}\right)^{1/3}}{1-\left(\frac{\Phi_s}{\Phi_{\text{pack}}}\right)^{1/3}}\right]. \tag{7}$$

Another popular approach, proposed by [18], consists in extending the dilute regime to the concentrated one in which the viscosity is expected to diverge when Φ_s tends to Φ_{pack},

$$\frac{\mu_m}{\mu_f} = \left(1-\frac{\Phi_s}{\Phi_{\text{pack}}}\right)^{-B\,\Phi_{\text{pack}}}, \tag{8}$$

where B is the Einstein's coefficient. The predictions of Eq. (7), represented by a pink dashed line in Fig. 5, clearly disagree with the present results, while Eq. (8) also cannot fit the measurements since the dependence of the exponent upon Φ_{pack} is in contradiction with the collapse of the results

involving samples characterized by different Φ_{pack}. Relaxing the constraint that the viscosity has to recover the value of that of the gas at low Φ_s, the following empirical expression, thus only relevant for the dense regime, fits well the experimental data:

$$\frac{\mu_m}{\mu_f} = 8.6\left(1 - \frac{\Phi_s}{\Phi_{\text{pack}}}\right)^{-0.45}. \tag{9}$$

Note that this scaling is relevant in the context of fluidization and sedimentation. This viscosity scale is expected to differ from the bulk viscosity determined in shearing suspensions, all the more so since the rheology of concentrated suspensions is known to be non-Newtonian [16], especially for elongated particles [19].

IV. CONCLUSION

To summarize, we explored the behavior of fine particles of random size and complex shape when fluidized by a hot gas in the Stokes flow regime. We considered three different materials, characterized by a *Group A* fluidization behavior [10], which allows the existence of a well-developed homogeneous regime between U_{mf} and U_{mb}, observed when $\phi_{\text{min}} < \phi_s < \phi_{\text{max}}$. Below ϕ_{min}, the stability of the uniform fluidized bed is broken by the nucleation of bubbles. Above ϕ_{max}, the bed remains aerated and rather behaves as a dry granular material dominated by particle-particle and particle-wall frictional interactions. The measured values of ϕ_{min} are close to 0.4 for the three considered materials, while those of ϕ_{max} significantly depend on their intrinsic properties and turn out to be related, in any case, to the packing value, such as $\phi_{\text{max}} \simeq 0.95\phi_{\text{pack}}$. Collecting the data of these three materials allowed us to investigate their fully fluidized homogeneous regime for a range of $\Phi_s/\Phi_{\text{pack}}$ from 0.65 to 0.95. In this context, no segregation develops and the fluidizing gas velocity is equal to the sedimentation velocity. Despite a wide range of particle size and shape distributions between the different samples, the evolution of the sedimentation velocities against the mixture volume fraction collapses into a single master curve provided that the velocity is scaled by $g(\rho_s - \rho_m)d^2/\mu_f$ and the volume fraction is normalized by its value at packing. The value of Φ_{pack}, which corresponds to the loose-packing state obtained when a previously fluidized suspension has freely settled down to the reservoir bottom, seems therefore to encapsulate all the information about the size and shape distributions required to reliably determine the sedimentation velocity of different samples. The present results are of primary interest for geophysical mass flows involving highly expanded suspensions of fine hot particles of complex random shape and size, such as pyroclastic flows, as well as for other common chemical engineering systems obtained in comparable environments.

[1] J. F. Richardson and W. N. Zaki, The sedimentation of a suspension of uniform spheres under conditions of viscous flow, Chem. Eng. Sci. **3**, 65 (1954).

[2] A. R. Abrahamsen and D. Geldart, Behaviour of gas-fluidized beds of fine powders part I. Homogeneous expansion, Powder Tech. **26**, 35 (1980).

[3] M. A. van der Hoef, M. Van Sint Annaland, N. G. Deen, and J. A. M. Kuipers, Numerical simulation of dense gas-solid fluidized beds: A multiscale modeling strategy, Annu. Rev. Fluid Mech. **40**, 47 (2008).

[4] R. H. Davis and A. Acrivos, Sedimentation of noncolloidal particles at low reynolds numbers, Annu. Rev. Fluid Mech. **17**, 91 (1985).

[5] É. Guazzelli and J. Hinch, Fluctuations and instability in sedimentation, Annu. Rev. Fluid Mech. **43**, 97 (2011).

[6] L. Girolami, Dynamics and sedimentation of laboratory-scale pyroclastic flows, Ph.D. thesis, University of Clermont II, 2008.

[7] L. Girolami, T. H. Druitt, O. Roche, and Z. Khrabrykh, Propagation and hindered settling of laboratory ash flows, J. Geophys. Res. **113**, B02202 (2008).
[8] L. Girolami, O. Roche, T. H. Druitt, and T. Corpetti, Particle velocity fields and depositional processes in laboratory ash flows, with implications for the sedimentation of dense pyroclastic flows, Bull. Volcanol. **72**, 747 (2010).
[9] L. Girolami, T. H. Druitt, and O. Roche, Towards a quantitative understanding of pyroclastic flows: Effects of expansion on the dynamics of laboratory fluidized granular flows, J. Volcanol. Geotherm. Res. **296**, 31 (2015).
[10] D. Geldart, Types of gas fluidization, Powder Tech. **7**, 285 (1973).
[11] J. L. P. Chen and D. L. Keairns, Particle segregation in a fluidized bed, Can. J. Chem. Eng. **53**, 395 (1975).
[12] S. Ergun, Fluid flow through packed colmuns, Chem. Eng. Prog. **48**, 89 (1952).
[13] L. Rondon, O. Pouliquen, and P. Aussillous, Granular collapse in a fluid: Role of the initial volume fraction, Phys. Fluids **23**, 073301 (2011).
[14] J. Happel and H. Brenner, *Low Reynolds Number Hydrodynamics*, with Special Applications to Particulate Media, Vol. 1 (Martinus Nijhoff, Dordrecht, 1983).
[15] E. J. Hinch, An averaged-equation approach to particle interactions in a fluid suspension, J. Fluid Mech. **83**, 695 (1977).
[16] S. P. Mueller, E. W. Llewellin, and H. M. Mader, The rheology of suspensions of solid particles, Proc. Royal Soc. A **466**, 1201 (2009).
[17] N. A. Frankel and A. Acrivos, On the viscosity of a concentrated suspension of solid spheres, Chem. Eng. Sci. **22**, 847 (1967).
[18] I. M. Krieger and T. J. Dougherty, A mechanism for non-Newtonian flow in suspensions of rigid spheres, Trans. Soc. Rheol. **3**, 137 (1959).
[19] F. Tapia, S. Shaikh, J. E. Butler, O. Pouliquen, and É. Guazzelli, Rheology of concentrated suspensions of non-colloidal rigid fibres, J. Fluid Mech. **827**, 725 (2017).